

Article

Comparison of LiDAR Operation Methods for Forest Inventory in Korean Pine Forests

Lan Thi Ngoc Tran ¹, Myeongjun Kim ^{1,*}, Hongseok Bang ¹, Byung Bae Park ² and Sung-Min Choi ³

¹ Forest Environment & Geospatial Technology Research Institute, Sejong 30084, Republic of Korea; tranlan1218@gmail.com (L.T.N.T.); redstone85@cnu.ac.kr (H.B.)

² Forest Resources Department, College of Agriculture and Life Science, Chungnam National University, Daejeon 34134, Republic of Korea; bbpark@cnu.ac.kr

³ Korea Forest Engineer Institute, Daejeon 35209, Republic of Korea; goodday@kfei.kr

* Correspondence: festri.kim@gmail.com; Tel.: +82-70-4151-3287

Abstract: Precise forest inventory is the key to sustainable forest management. LiDAR technology is widely applied to tree attribute extraction. Therefore, this study compared DBH and tree height derived from Handheld Mobile Laser Scanning (HMLS), Airborne Laser Scanning (ALS), and Integrated ALS and HMLS and determined the applicability of integrating HMLS and ALS scanning methods to estimate individual tree attributes such as diameter at breast height (DBH) and tree height in pine forests of South Korea. There were strong correlations for DBH at the individual tree level ($r > 0.95$; $p < 0.001$). HMLS and Integrated ALS-HMLS achieved high accuracy for DBH estimations, showing Root Mean Squared Error (RMSE) of 1.46 cm (rRMSE 3.7%) and 1.38 cm (rRMSE 3.5%), respectively. In contrast, tree height obtained from HMLS was lower than expected, showing an RMSE of 2.85 m (12.74%) along with a bias of -2.34 m. ALS data enhanced the precision of tree height estimations, achieving a RMSE of 1.81 m and a bias of -1.24 m. However, integrating ALS and HMLS data resulted in the most precise tree height estimations resulted in a reduced RMSE to 1.43 m and biases to -0.3 m. Integrated ALS and HMLS and its advantages are a beneficial solution for accurate forest inventory, which in turn supports forest management and planning.



Academic Editors: Pablito M. López-Serrano and Marín Pompa-García

Received: 17 March 2025

Revised: 29 March 2025

Accepted: 2 April 2025

Published: 7 April 2025

Citation: Tran, L.T.N.; Kim, M.; Bang, H.; Park, B.B.; Choi, S.-M. Comparison of LiDAR Operation Methods for Forest Inventory in Korean Pine Forests. *Forests* **2025**, *16*, 643. <https://doi.org/10.3390/f16040643>

Copyright: © 2025 by the authors. Licensee MDPI, Basel, Switzerland. This article is an open access article distributed under the terms and conditions of the Creative Commons Attribution (CC BY) license (<https://creativecommons.org/licenses/by/4.0/>).

Keywords: airborne laser scanning; handheld mobile laser scanning; point cloud density; point cloud registration; forest inventory

1. Introduction

Forest inventories play a critical role in sustainable forest management and various ecosystem services [1,2]. Traditional field surveys measure tree location, species, DBH, and tree height [3–8]; however, parameters such as crown diameter and crown length are not often considered [9]. Moreover, the introduction of Light Detection and Ranging (LiDAR) technology has opened a new era in the forestry field and has been applied to forestry investigation since the early 1980s [3,10–12]. Its distinctive features provide potential to enhance productivity in forest inventory by substituting traditional manual methods of measuring tree attributes with more automated processes through 3D point clouds with high accuracy even at individual tree levels [4,13,14]. In addition, LiDAR mapping proves to be particularly advantageous when a project necessitates precise elevation information for densely vegetated regions, expansive terrains, or locations that are hard to reach or pose safety hazards for ground access [15]. LiDAR technology can be categorized into three main types: (1) space-borne LiDAR, encompassing systems like Unmanned Aerial Vehicle

(UAV) LiDAR and airborne laser scanning (ALS); (2) ground-based LiDAR, which includes terrestrial laser scanning (TLS); and (3) mobile LiDAR, featuring options such as handheld mobile laser scanning (HMLS) and backpack mobile laser scanning (BMLS) [16].

Airborne laser scanning (ALS) is a technology that combines a laser scanning device with a global navigation satellite system (GNSS) or an inertial measurement unit (IMU) to achieve accurate positioning and orientation [17]. A significant benefit of ALS is its ability to assess the height of tree canopies and the tops of trees from an aerial perspective on a broad scale [17–19]. On the other hand, numerous studies have stated that a significant limitation of using ALS in operations is its inability to capture complicated structures beneath the canopy [20–22]. After collecting data using ALS, one of the most common methods for estimating tree height is through the creation of a Canopy Height Model (CHM) that yields a raster dataset where each pixel value corresponds to the height of the vegetation at that location [23,24]. The CHM is calculated by taking the difference between the ground elevation, represented by the Digital Elevation Model (DEM), and the elevation of the vegetation canopy, indicated by the Digital Surface Model (DSM) [25,26]. Algorithms like watershed segmentation based on CHM or local maxima detection are used to identify individual trees [22]. Therefore, the CHM method is considered a feasible approach for estimating tree heights [1].

Over the past several decades, terrestrial laser scanning (TLS) has been utilized in the field of forestry [27]. TLS includes ground-based laser scanning and handheld mobile laser scanning (HMLS) conducted by an operator to gather a highly detailed point cloud in a dynamic way [17]. Since HMLS can capture the finer detail beneath the canopy, besides DBH and height, it also permits the estimation of additional inventory parameters (e.g., crown diameter, stem straightness, and foliage biomass) [4,28]. However, HMLS also has challenges when identifying treetops in high and thick canopies or dense understory vegetation [1,9,17]. The heights of trees obtained from HMLS point cloud data are frequently lower than those measured in the field, primarily because of the overlapping canopies of the individual trees [4,10,14,29,30].

Handheld and airborne LiDAR technologies both characterize stand structure through point cloud data. However, while handheld LiDAR examines the canopy from a bottom-up approach, airborne LiDAR systems capture a top-down view of the canopy [2,5]. Because items that are closer to the device usually produce a recognizable return, point clouds collected through airborne laser scanning reveal the upper sections of the canopy, whereas those gathered via handheld laser scanning highlight the lower portions of the tree crowns [2,21]. Therefore, the integration of HMLS and ALS is described as the best approach to simulate the structure beneath the canopy as well as the upper canopy [21,31]. In this paper, we aimed to compare DHB and tree height obtained using HMLS, ALS, and Integrated ALS-HMLS using field surveys as a benchmark in the pine forest of Pocheon-si, Republic of Korea. Specifically, we highlight the advantages of combining ALS and HMLS in forest attribute extraction compared to applying a single approach.

2. Materials and Methods

2.1. Study Area

The study area, which has a coverage of 1.6 ha, is a coniferous planted *Pinus koraiensis* forest in Pocheon-si, Gyeonggi-do, Republic of Korea (latitude 37°45′58.58″ N; longitude 127°10′36.01″ E) (Figure 1). The annual precipitation is about 1272.4 mm with a mean temperature of 11.2 °C, the highest temperature is 17.6 °C, and lowest temperature is 5.5 °C (2011~2020) (Meteorological Data Open Portal, Korea (kma.go.kr)). Its topography is relatively gentle, with elevation varying from 154 m to 190 m above sea level.

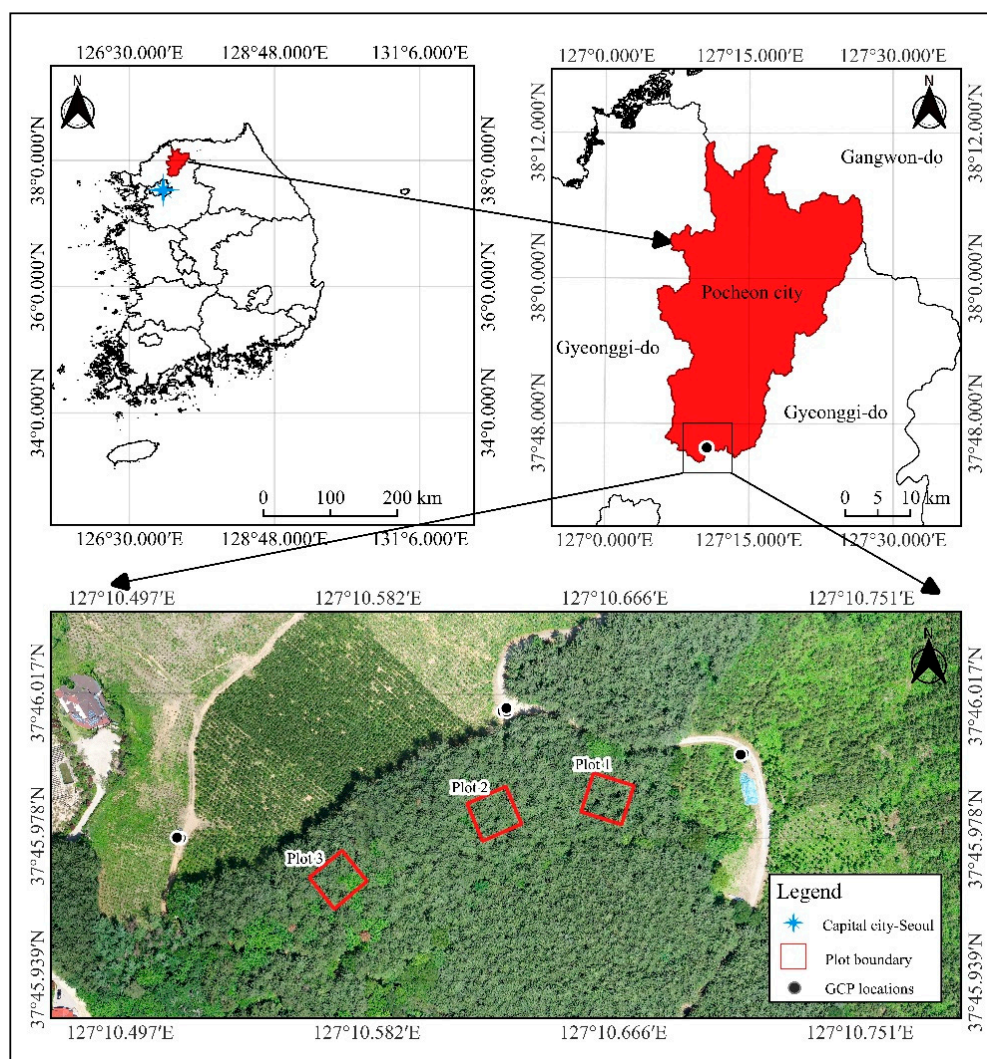


Figure 1. General view of the study area and plot locations.

2.2. Data Collection

2.2.1. Field Measurement (FM)

Field measurements were conducted from 28 to 29 May 2024, primarily following the forest sampling methodology outlined in Practical Forest Measurement and Survey by the National Institute of Forest Science, South Korea [32]. First, three plots (20 m × 20 m) were established in the upper, central, and lower sections of the research area. Within these plots, only *Pinus koraiensis* was selected as the dominant species for measurement purposes (Table 1). The herbaceous and shrub areas were regarded as the understory layer. Tree DBH was measured at 1.20 m above ground using a fiberglass diameter tape (SL05001, Shinil Science Co., Ltd., Paju-si, Republic of Korea). Tree height was calculated using Vertex IV (Haglöf Sweden AB, Långsele, Sweden). All measured trees were marked with labels. Then, collected data, including tree locations, were recorded in inventory form presented by the NIFS.

Table 1. Description of tree attributes from field measurement in three plots. The standard deviation for the sample is indicated within parentheses.

Attributes	Plot 1	Plot 2	Plot 3
Min DBH (cm)	29.2	23.1	36.5
Max DBH (cm)	46.8	57.9	62.8
Mean DBH (cm)	36.88 (4.63)	39.14 (8.03)	43.01 (7.37)
Min tree height (m)	16.2	20.3	18.0
Max tree height (m)	23.8	25.4	25.9
Mean tree height (m)	21.15 (2.35)	22.66 (2.31)	22.09 (1.89)
Plot size (m ²)	400	400	400
No. of trees (#)	14	17	11
Tree density (tree/ha)	350	425	275
Basal area (m ²)	0.61	0.83	0.65

2.2.2. Handheld Mobile Laser Scanning (HMLS)

Point cloud data scanning was conducted from 28 to 29 May 2024 in the field using a handheld ZEB Horizon scanner (GeoSLAM Ltd., Nottingham, UK) (Table 2) carried by a forest surveyor (Figure 2A). The sensor emits continuous laser beams that scatter as near-infrared rays with a wavelength of 905 nm [33]. The surrounding objects respond to this by reflecting the emitted pulses. Then, the sensor calculates the distance between objects and captures their angles in a two-dimensional (2D) format. Simultaneously, a SLAM algorithm integrates the 2D profiles with data from the IMU to create 3D point clouds without using a GNSS receiver [27,33].

Table 2. Specification of ZEB Horizon.

Features	Description
Range	100 m
Laser	Class 1/λ 903 nm
FOV	360° × 270°
Scanner points per second	300,000
No. of sensors	16
Vertical angular resolution	2°
Horizontal angular resolution	0.2°
Raw data file size	25–50 MB/min
Relative accuracy	Up to 6 mm
Range sensor	Velodyne VLP-16
Range rating	Class 1 Eye-Safe
POS system	Integrated SLAM system
Operating time	3 h
RGB camera	CAM

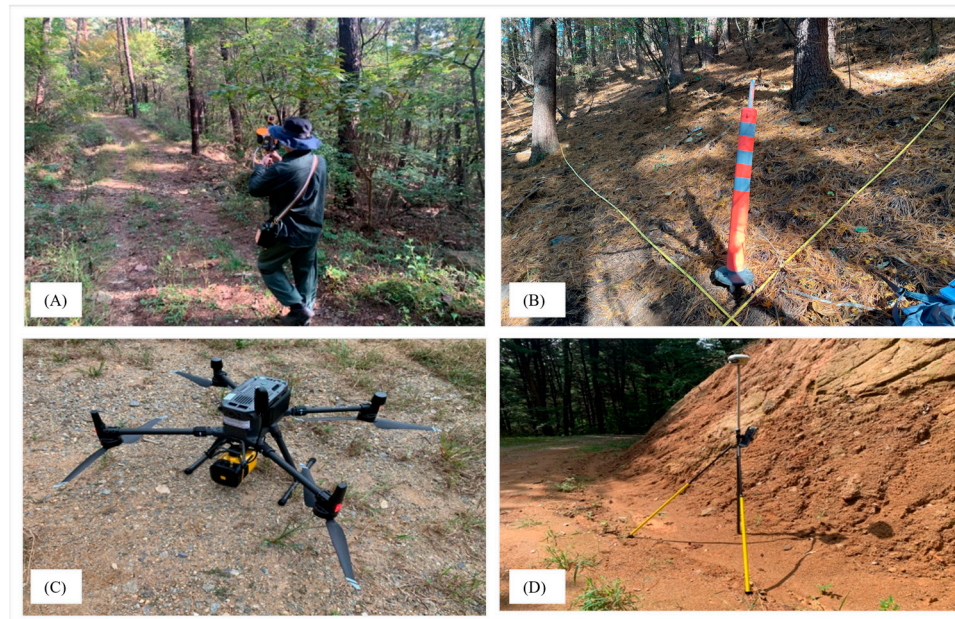


Figure 2. ALS and HMLS data collection: (A) handheld mobile laser scanning; (B) pole at 4 corners of the plots; (C) airborne laser scanner mounted on a drone; (D) static base station on the ground.

Before HMLS data acquisition, the plot center and four corners of the plots were marked by four poles (0.7 m length; Figure 2B) to help the data analyst quickly identify the plot position and plot boundary when clipping the sample plot on a 3D point cloud). In addition, two cars were placed on the border of the study area under an open-spaced area to use as identified objects for data registration of handheld and airborne LiDAR point clouds. A parallel walking cross plot at a consistent distance was performed to achieve the maximum number of loops, and the loop was completed by returning to the initial position. Plots were scanned slowly at a speed of 1 m/s with stable movement to guarantee both point cloud quality data and its coverage [33].

2.2.3. Airborne Laser Scanning (ALS)

Airborne point cloud data were acquired on 29 May using a LiDAR scanner (YellowScan, Saint-Clément-de-Rivière, France) mounted on a Matrice 300 RTK drone (DJI Enterprise, Shenzhen, China) (Figure 2C). The UAV flight measurement covers about 1.5 ha. The flight was conducted two times at different altitudes (100 m and 70 m above ground level) with side overlaps of 80%. A base station and seven Ground Control Points (GCPs) were distributed within the area to receive satellite positioning data and send them to a GNSS receiver (Figure 2D). Precise coordinates were added to point cloud data using POSPAC, and then a complete point cloud was created using CloudStation software v.2403.0.1 (YellowScan, Saint-Clément-de-Rivière, France). For reference use purposes, an RGB image was also acquired using a DJI Phantom 4 Pro quadcopter UAV (DJI Enterprise, Shenzhen, China), and then an orthophoto of the study site was obtained using UAS Applications Master v13.2.3 (Trimble, Stuttgart, Germany).

2.3. Point Cloud Data Analyses

2.3.1. HMLS

HMLS point clouds were filtered using the Statistical Outlier Removal (SOR) algorithm in LiDAR360 to remove noise points caused by wind and multipath effects. Smooth points based on moving least squares were used to make the point cloud look more consistent. Normalization was performed to eliminate the effect of terrain elevation on LiDAR height.

Then, the point cloud was sliced at 1.2 m from the ground using the Filter by Elevation function. Tree DBH was manually selected using a least-squares circular fitting algorithm to fit the circle from x-y coordinates in 2D environments (Figure 3A) and can be seen in 3D environments (Figure 3B). Seed points were then used as input for point cloud segmentation, which adopted individual tree segmentation algorithms from the study of Li et al. (2012) [34]. Visual inspection was subsequently conducted to correct the possible segmentation mistakes found in the point cloud of individual trees (Figure 3C). All analyses were conducted in LiDAR360 software version 5.4 (GreenValley International, Berkeley, CA, USA).

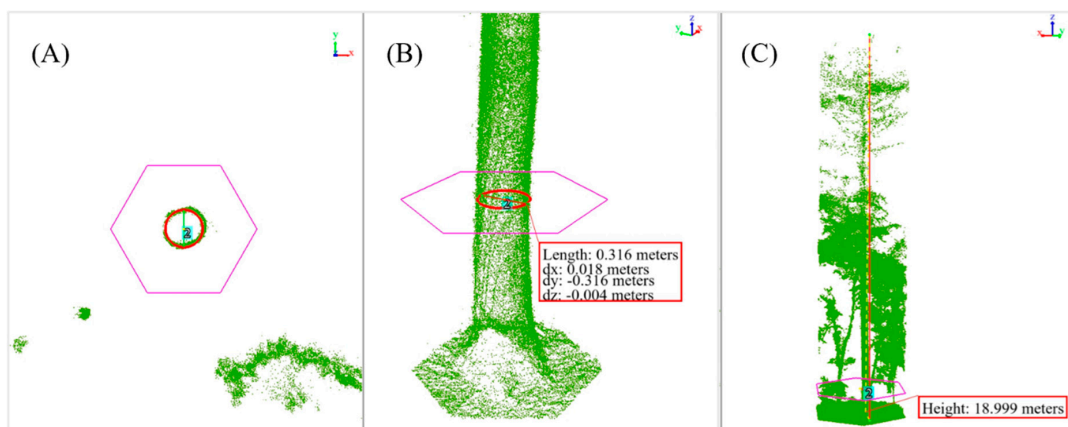


Figure 3. Tree DBH measurement in 2D (A) and 3D (B) and visual inspection of tree height from HMLS (C).

2.3.2. ALS

For the ALS point cloud, Remove Outliers and Smooth Points were also applied. First, a classification algorithm that operates automatically was utilized to separate the point cloud into ground points and vegetation points. Ground points were interpolated into the DEM using an Inverse Distance Weighting (IDW) interpolation method (Figure 4A). For the DSM, a similar grid-based interpolation approach was applied to generate the surface capturing the vegetation canopy (Figure 4B). A Canopy Height Model (CHM) was created by subtracting the DSM from the DEM according to the method of Douss et al. (2022) [25]. Then, CHM segmentation based on the basic principle of the watershed segmentation algorithm was performed to provide insights into vegetation height and structure (Figure 4C). The pixel size was 10 cm \times 10 cm for all raster data.

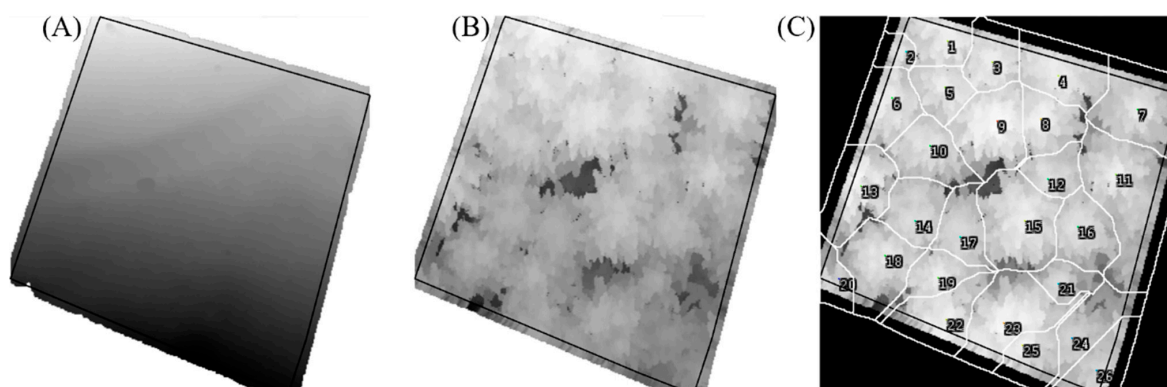


Figure 4. Example of CHM results including DEM (A), DSM (B), and CHM (C).

2.3.3. ALS and HMLS Registration

ALS and HMLS point clouds were registered in Trimble RealWorks Advanced-Plant[®] 11.0 version (Trimble, Stuttgart, Germany) with the cloud-based registration function using artificial objects (e.g., cars) to register two-point clouds. First, coarse registration that roughly registered two point clouds, including the point cloud from ALS containing local coordinate systems (Korea 2002/ Central Belt 2010, EPSG: 5186), served as references, and the point cloud from HMLS was a moving cloud. Then, fine registration was conducted through supervised visual selection of three point pairs extracted from artificial objects (car) and tree. As a result, the achieved accuracy of point cloud registration was 2 cm (Figure 5).

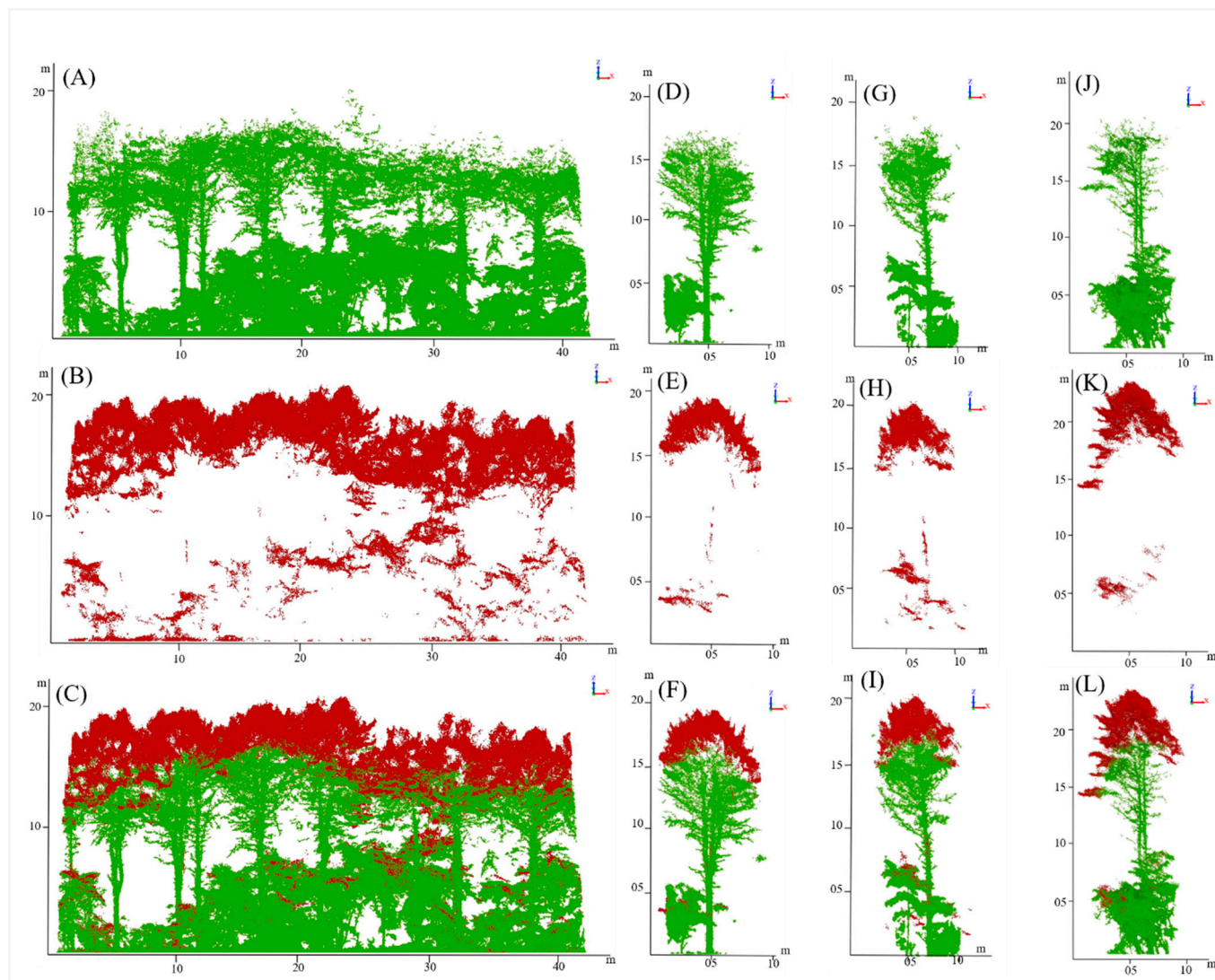


Figure 5. Result of ALS and HMLS registration (C,F,I,L). Forest point cloud acquired from HMLS (A), ALS (B), and Integrated ALS-HMLS (C); individual tree in Plot 1 acquired from HMLS (D), ALS (E), and Integrated ALS-HMLS (F); individual tree in Plot 2 acquired from HMLS (G), ALS (H), and Integrated ALS-HMLS (I); individual tree in Plot 3 acquired from HMLS (J), ALS (K), and Integrated ALS-HMLS (L). The green color represents the HMLS approach; the red color represents the ALS approach.

2.3.4. Density Assessment

To calculate the point density of ground and vegetation subsets from a point cloud, the following methodology was employed. First, the LiDAR point cloud data were pre-processed to ensure accuracy and uniformity, including noise removal and coordinate system

verification. Next, the data were classified into ground and vegetation points using an automated classification algorithm in LiDAR360, which assigns points to specific categories based on their height and spatial characteristics. Once the classification was complete, the dataset was divided into two subsets: ground points and vegetation points. Each subset was processed independently to compute point density. A grid-based approach was utilized, wherein the region of interest was divided into uniform grid cells of a predefined size (1 m × 1 m). For each subset, the total number of points falling within each grid cell was counted, and the density was calculated as the number of points per unit area (points/m²).

2.4. Accuracy Assessment

The Shapiro–Wilk test was used to determine the normal distribution of DBH and tree height. Then, Pearson’s correlation analysis was applied to normally distributed data while data without normality were subjected to Spearman’s correlation analyses. Moreover, a paired samples t-test was utilized to assess whether there were any notable differences in tree diameter at breast height (DBH) and tree height as measured using three different methods. The accuracy assessment was additionally conducted using Root Mean Squared Error (RMSE), relative RMSE (rRMSE), bias, relative bias (rBias), and Mean Absolute Error (MAE), with the field measurements used as the reference data, represented by Equations (1) to (5) [6]. Consequently, any potential linear relationships were examined visually. All statistical analyses were conducted using SPSS software, v.29 adhering to a significance level of less than 5%.

$$RMSE = \sqrt{\frac{\sum_{i=1}^n (\hat{y}_i - y_i)^2}{n}} \quad (1)$$

$$rRMSE = \frac{RMSE}{y_m} \times 100 \quad (2)$$

$$Bias = \left(\frac{\sum_{i=1}^n e_i}{n} \right) \quad (3)$$

$$rBias = \frac{Bias}{y_m} \times 100 \quad (4)$$

$$MAE = \frac{1}{n} \sum_{i=1}^n |\hat{y}_i - y_i| \quad (5)$$

where \hat{y}_i is the DBH value extracted from HMLS, y_i is the DBH measured in the field, n is the number of trees in each plot, e_i is the error term, y_m is the mean of the field survey, and i is the sample index.

The workflow presented in Figure 6 shows the methodology used in this study.

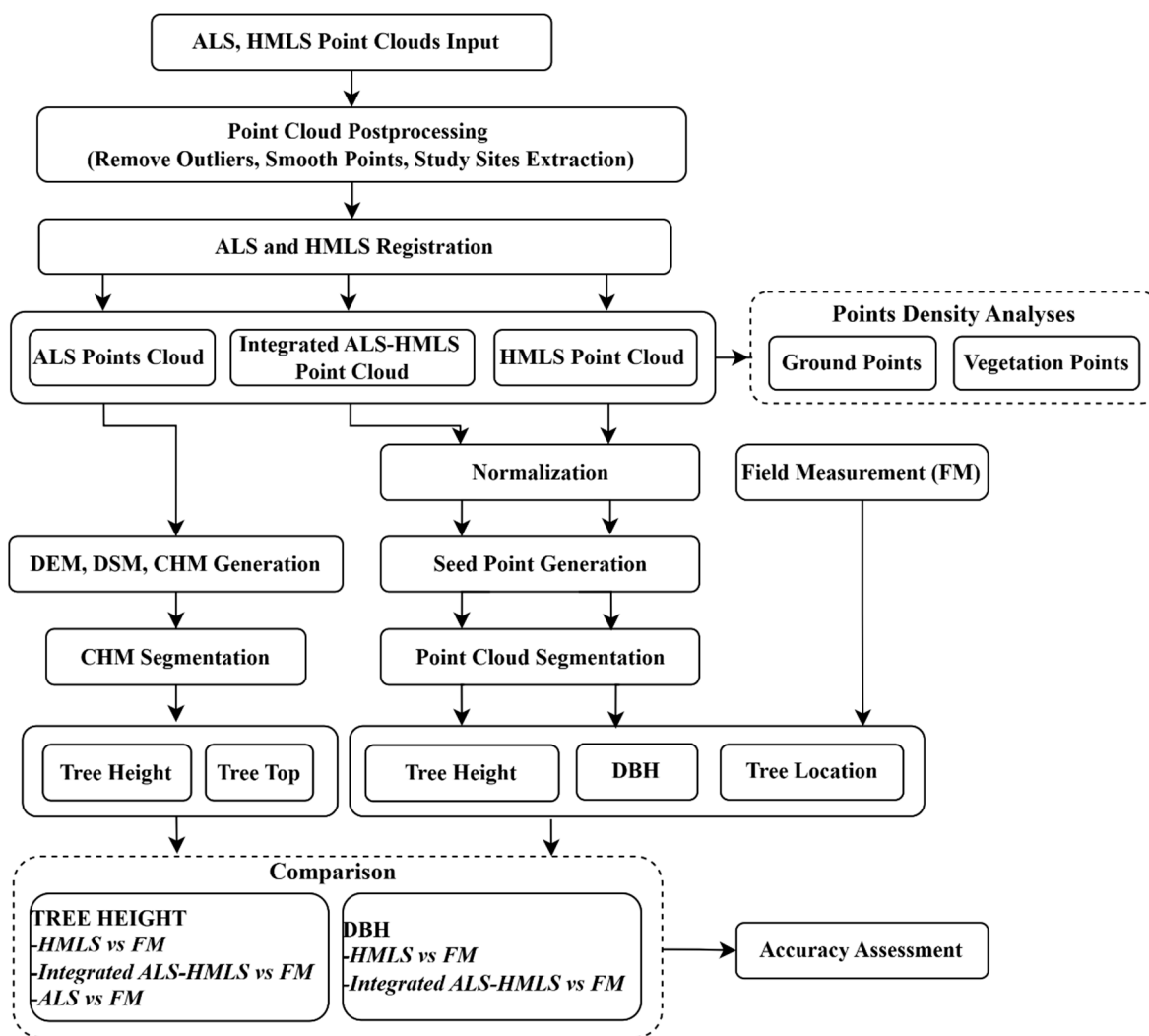


Figure 6. Flowchart for data processing.

3. Results

3.1. Point Cloud Density Analyses

Point cloud density (points/m²) for both ground and vegetation across the three plots, measured through ALS, HMLS, and Integrated ALS-HMLS, are shown in Table 3.

Table 3. Point cloud density of ground and vegetation point clouds classified from ALS, HMLS, and Integrated ALS-HMLS.

Point Clouds	Plot	ALS	HMLS	Integrated ALS-HMLS
Ground (points/m ²)	Plot 1	16	3389	3393
	Plot 2	13	2468	2470
	Plot 3	15	1157	1167
Vegetation (points/m ²)	Plot 1	2398	21,315	23,710
	Plot 2	2683	26,727	29,129
	Plot 3	2793	23,594	26,356

Ground points extracted from point clouds are important for DEM generation and other analyses. Regarding ground point density, the data indicated that ALS consistently recorded the lowest density (between 13 and 16 points/m²) among all plots compared to

HMLS. On the other hand, HMLS revealed a significant increase in ground point density, with measurements between 1157 and 3389 points/m². The combination of ALS and HMLS resulted in a minor enhancement, producing values ranging from 1167 to 3393 points/m². However, a very low ground point density was shown in ALS (avg. 11 points/m²), which demonstrates the limited capability of ALS in capturing ground-level details. Compared to ALS, HMLS exhibits a much higher resolution of ground surfaces (avg. 2338 points/m²). This underscores its superior capability in resolving vegetation structures. This integration offers moderate improvements compared to HMLS, suggesting a complementary effect of ALS in refining the results.

In terms of vegetation, ALS presents the lowest point densities, which lie between 2398 and 2793 points/m², reflecting its limited capacity to capture intricate details of vegetation. HMLS, however, experiences a notable escalation, with densities recorded between 21,315 and 26,727 points/m². The Integrated ALS-HMLS approach further boosts vegetation point densities, reaching the highest values across all plots, between 23,710 and 29,129 points/m². HMLS significantly outperforms ALS in capturing both ground and vegetation densities, demonstrating its efficacy for detailed point cloud generation. The Integrated ALS-HMLS method provides incremental improvements over HMLS, emphasizing the advantage of combining the strengths of both ALS and HMLS methods.

3.2. Diameter at Breast Height (DBH)

Table 4 indicates average DBH values estimated using the HMLS and Integrated ALS-HMLS approaches and their test results. As seen in Table 4, the two approaches (HMLS and Integrated ALS-HMLS) showed highly positive correlated DBH measurements, with statistically significant correlations in all cases ($r > 0.93$, $p < 0.001$). The normality test showed that the DBH values were normally distributed ($p > 0.05$) in Plot 1 and Plot 2 but not in Plot 3 and the overall dataset ($p < 0.05$).

Table 4. Test results and mean DBH measured using the two approaches. The number in parentheses represents the standard deviation.

Plot	Approaches	Mean DBH	<i>p</i> -Value (Normality Test)	<i>r</i> Coefficient	<i>p</i> -Value (Correlation)
1	HMLS	36.22 (4.85)	0.809	0.954	<0.001
	Integrated ALS-HMLS	35.97 (4.44)	0.452	0.982	<0.001
2	HMLS	37.85 (7.76)	0.474	0.993	<0.001
	Integrated ALS-HMLS	37.98 (8.11)	0.542	0.991	<0.001
3	HMLS	42.34 (7.02)	0.002	0.952	<0.001
	Integrated ALS-HMLS	42.52 (7.1)	0.007	0.936	<0.001
All	HMLS	38.48 (6.99)	0.013	0.975	<0.001
	Integrated ALS-HMLS	38.5 (7.13)	0.015	0.977	<0.001

Figure 7 displays scatterplots comparing the diameter at breast height (DBH) measurements obtained from field measurements (FM) with HMLS and Integrated ALS-HMLS remote sensing approaches. Figure 7 demonstrates that both HMLS and Integrated ALS-HMLS approaches yield DBH measurements strongly correlated with field measurements. Regression equations indicate that both remote sensing methods provide accurate and reliable estimations of DBH, with minor differences in slope and intercept adjustments. These results validate the effectiveness of the remote sensing approaches for DBH measurement.

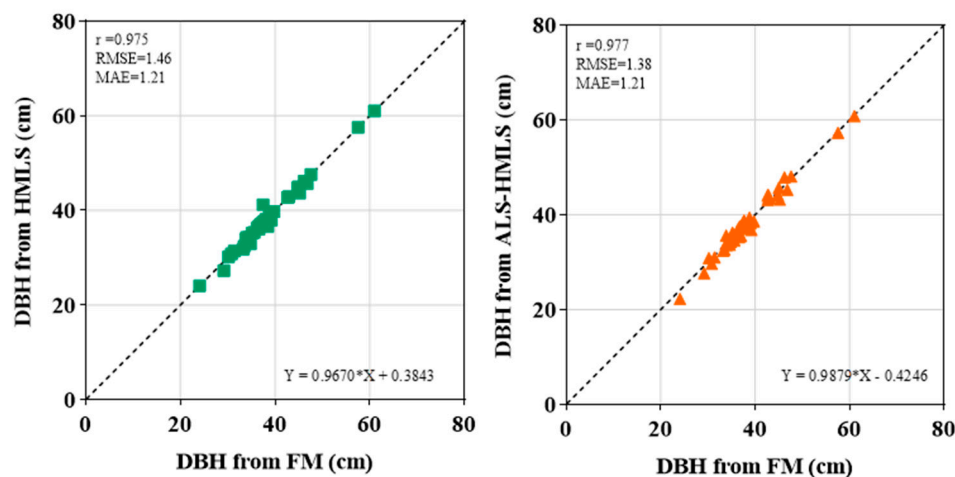


Figure 7. Comparison of DBH acquired from HMLS and Integrated ALS and HMLS approaches using field measurement (FM) as a benchmark.

Table 5 presents an evaluation of the accuracies of the two methods. Plot 3 achieved the most precise estimation of DBH, utilizing the HMLS method, with the lowest values for RMSE (1.10 cm) and MAE (0.91 cm). In contrast, Plot 1 reflects a moderate level of accuracy; however, it reports a slightly elevated RMSE of 1.54 cm and a bias of -0.66 cm. Plot 2 exhibits a higher RMSE of 1.59 cm and a bias of -1.28 cm, suggesting that it has less alignment with field measurements. All estimations displayed a negative bias, indicating that the HMLS method’s DBH measurements were smaller than those obtained through manual field measurements.

Table 5. Accuracies of DBH estimation using HMLS.

Plot	Approaches	RMSE (cm)	rRMSE (%)	Bias (cm)	rBias (%)	MAE (cm)
1	HMLS	1.54	4.18	-0.66	-1.79	1.23
	Integrated ALS-HMLS	1.54	4.18	-0.66	-1.79	1.23
2	HMLS	1.59	4.05	-1.28	-3.28	1.40
	Integrated ALS-HMLS	1.59	4.06	-1.16	-2.98	1.27
3	HMLS	1.10	2.55	-0.68	-1.58	0.91
	Integrated ALS-HMLS	1.18	2.74	-0.48	-1.13	1.04
All	HMLS	1.46	3.70	-0.92	-2.33	1.21
	Integrated ALS-HMLS	1.38	3.50	-0.90	-2.29	1.21

3.3. Height

Table 6 reveals that the Integrated ALS-HMLS method consistently yields the highest average tree height estimates across all plots, reaching an overall mean of 23.03 m, followed by ALS at 21.09 m and HMLS at 19.99 m. Although ALS and Integrated ALS-HMLS demonstrate moderate correlations with field measurements, particularly noticeable in Plots 2 and 3, the correlations observed for HMLS are generally weaker. The results of the normality test indicate that the HMLS approach in Plot 1 and the complete dataset do not conform to normal distribution. These results imply that Integrated ALS-HMLS and ALS are more dependable and consistent in estimating tree heights when compared to HMLS.

Table 6. Test results and mean tree height measured using the three approaches. The numbers in parentheses represent the standard deviation.

Plot	Approaches	Mean Height	p-Value (Normality Test)	r Coefficient	p-Value (Correlation)
1	HMLS	19.76 (1.74)	0.039	−0.191	0.514
	Integrated ALS-HMLS	21.69 (1.36)	0.245	0.186	0.524
	ALS	20.71 (1.01)	1.000	0.217	0.456
2	HMLS	20.27 (0.9)	0.984	0.684	0.003
	Integrated ALS-HMLS	22.47 (1.01)	0.135	0.586	0.014
	ALS	21.78 (1.36)	0.333	0.511	0.036
3	HMLS	19.86 (1.01)	0.228	0.757	0.007
	Integrated ALS-HMLS	21.8 (1.37)	0.086	0.650	0.030
	ALS	20.52 (1.08)	0.263	0.860	0.001
All	HMLS	19.99 (1.26)	0.009	0.339	0.028
	Integrated ALS-HMLS	22.03 (1.28)	0.190	0.518	0.000
	ALS	21.09 (1.29)	0.187	0.573	<0.001

The tree height estimation from HMLS and Integrated HMLS and ALS are compared to reference field measurement data in Figure 8. The chart displays the precision metrics for tree height estimation across three different plots utilizing HMLS, Integrated ALS-HMLS, and ALS in comparison with the reference data.

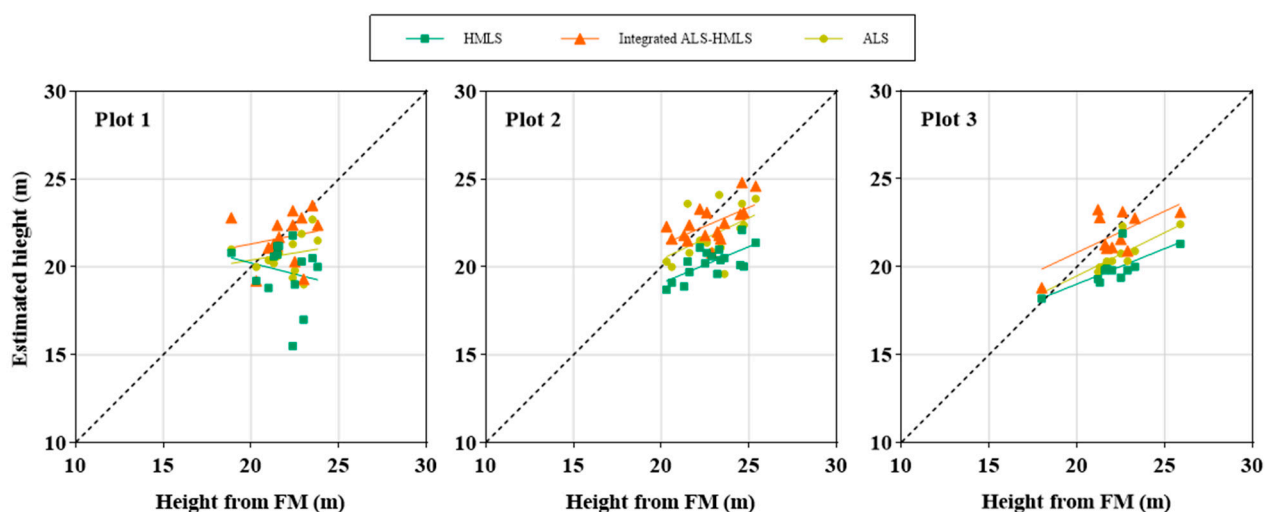


Figure 8. Comparison of tree height estimations at plot level from field measurements against HMLS, ALS, and Integrated ALS-HMLS.

Under the HMLS methodology, tree height was significantly underestimated, resulting in an RMSE of 5.13 m and an MAE of 4.75 m, as displayed in Table 7. Conversely, when HMLS was integrated with ALS, there was an enhancement in bias and other precision indicators, including an RMSE of 1.56 m and an MAE of 1.25 m. At the level of individual plots, HMLS exhibited the highest RMSE, varying from 2.55 to 3.13 cm, with a bias range of 2.14 to 2.57 cm and MAE values lying between 2.26 and 2.57 cm, closely followed by ALS. In stark contrast, the combined ALS-HMLS approach produced the most advantageous outcomes, achieving the lowest RMSE of 1.66 cm for both bias and MAE. Overall, the Integrated ALS-HMLS method achieved the best accuracy, marked by a minimum RMSE

of 1.43 cm, a relative root mean square error of 6.41%, a bias of -0.30 cm, and an MAE of 1.10 cm. While ALS demonstrated moderate performance, it recorded higher error levels with an RMSE of 1.81 cm and a bias of -1.24 cm compared to the Integrated ALS-HMLS approach. Meanwhile, HMLS showed the highest levels of error and an underestimation, reaching a peak RMSE of 2.85 cm, accompanied by a bias of -2.30 cm. The negative bias implies that the estimates provided by all three methods fell short of the actual reference values.

Table 7. Accuracy assessment of tree height estimation from HMLS, ALS, and Integrated ALS-HMLS.

Plot	Approaches	RMSE (cm)	rRMSE (%)	Bias (cm)	rBias (%)	MAE (cm)
1	HMLS	3.13	14.31	-2.14	-9.78	2.41
	Integrated ALS-HMLS	1.66	7.57	-0.21	-0.98	1.04
	ALS	1.85	8.46	-1.18	-5.41	1.49
2	HMLS	2.78	12.15	-2.57	-11.25	2.57
	Integrated ALS-HMLS	1.23	5.37	-0.36	-1.60	1.08
	ALS	1.73	7.57	-1.06	-4.66	1.45
3	HMLS	2.55	11.55	-2.23	-10.08	2.26
	Integrated ALS-HMLS	1.40	6.36	-0.29	-1.33	1.19
	ALS	1.89	8.58	-1.57	-7.12	1.70
All	HMLS	2.85	12.74	-2.34	-10.47	2.44
	Integrated ALS-HMLS	1.43	6.41	-0.30	-1.33	1.10
	ALS	1.81	8.13	-1.24	-5.54	1.53

4. Discussion

4.1. Point Cloud Density

Point cloud density is one of the most important parameters in LiDAR data analyses [35]. In this study, the differences in point cloud densities among ALS, HMLS, and integration of ALS and HMLS were determined to demonstrate the strengths and limitations of each approach. According to Balsa et al. (2012), ALS consistently records the lowest point densities, particularly for ground points, due to its airborne scanning characteristics [35]. With a larger footprint and lower resolution at ground level, ALS struggles to capture fine-scale details, leading to sparse point distributions [36,37]. In addition, this limitation impacts its ability to extract precise terrain features, which are essential for applications such as digital elevation model (DEM) generation and forest structure analysis [38].

In contrast, HMLS exhibits significantly higher densities for both ground and vegetation points because of the close range and high-resolution scanning capabilities of the technology [27]. By capturing a higher level of detail, HMLS enhances the accuracy of point cloud-based analyses, particularly in complex forest environments where high-density data is crucial for structural assessments [39]. The substantial increase in ground point density compared to ALS indicates that HMLS is more effective in capturing detailed terrain features, making it a valuable tool for applications requiring fine-resolution point clouds [40]. Similarly, for vegetation, the higher density from HMLS provides a more comprehensive representation of tree trunks, which is critical for biomass estimation and ecological modelling [41].

The integration of ALS and HMLS in this study offers an optimal balance between broad coverage and high detail capture, resulting in improved overall point densities. Panagiotidis et al. (2022) recorded similar results in that the fusion of an airborne laser scanning and static terrestrial laser scanning maximized the accumulation of point clouds [42]. By leveraging ALS's capability to cover large areas efficiently and HMLS's ability to provide detailed local measurements, the integrated approach enhances data completeness, especially in tree height estimation in this study. This approach makes ALS-HMLS integration the most effective method for capturing both ground and vegetation features, as it mitigates the individual limitations of each technique while maximizing their advantages, as validated in a study by Lee et al. (2022) [43]. Consequently, the combined approach holds significant potential for improving forest inventory accuracy, terrain modelling, and vegetation characterization [4,6,10].

4.2. Tree DBH

Our study results show that the combination of ALS and HMLS did not enhance the accuracy of DBH estimation. For example, the average DBH calculated from HMLS (38.48 cm) was very similar to that derived from the combined HMLS and ALS approach (38.5 cm). The study further demonstrates that HMLS is a promising approach for assessing tree DBH, achieving a notable accuracy with an RMSE of 1.46 cm ($rRMSE = 3.7\%$) across all study plots. Similar findings were reported in previous research that assessed DBH within the range of 1 cm to 3.3 cm in conifer forests in Italy [4] and Japan [6] and Scots pine forests in Finland [44]. The outcomes from this study were close to what was found in the Yunnan pine forest (RMSE = 1.17 cm) in China [29]. Additionally, the mean absolute error was identical for HMLS and integrating ALS and HMLS approaches (MAE = 1.21 cm), indicating that ALS did not contribute to DBH due to its limitations in capturing detail beneath the canopy. However, in a past study by Panagiotidis et al. (2022), airborne laser scanning was reported to overestimate the DBH in oak and spruce forests in Italy [42]. Because the tree trunks of oaks and spruces in this study were captured well due to the absence of an understory, the bias values for DBH measurements obtained from HMLS and Integrated ALS-HMLS were negative and approximately equal to 1, -0.92 , cm and -0.9 cm, respectively (Table 5). This finding illustrates that the DBH estimated from LiDAR technology in this study was unbiased and smaller than the field measurement data. This bias aligns with earlier studies by Gianneti et al. (2018) [4], who reported a bias of -0.38 cm using a handheld ZEB1 in Mediterranean forest stands, and Bauwens et al. (2016) [9], who reported a very small bias of -0.08 cm. As shown in Figure 9, the random positive and negative variances in the DBH predictions displayed a consistent trend near the zero levels, indicating that the calculated DBHs were typically free from bias.

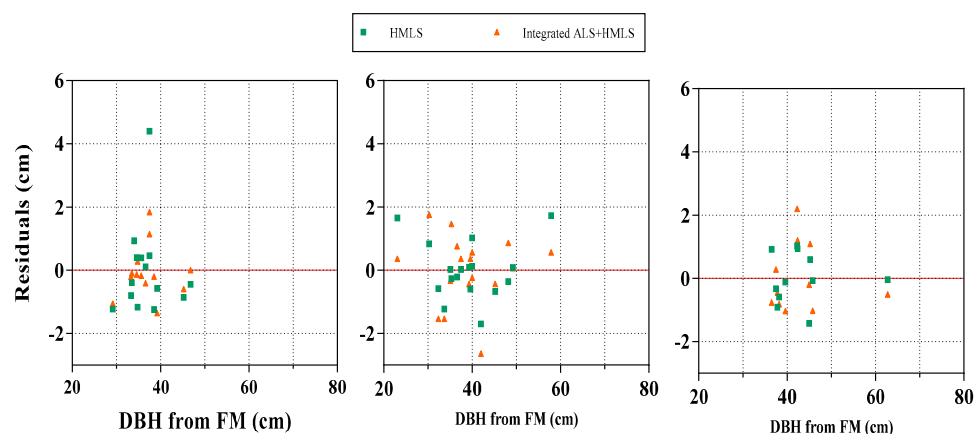


Figure 9. Residual plots of tree DBHs in each plot. Zero lines are highlighted in red.

4.3. Tree Height

Tree height measurements using HMLS data in this study resulted in a significant underestimation. The study corresponds with results from Lee et al. (2022), who compared tree height from Integrated ALS and HMLS with ground truth with an RMSE of 2 m [43]. Additionally, a similar study conducted in Taebek reported an RMSE of 3.297 m, an MAE of 2.303 m, and a bias of -1.905 m [45]. However, the RMSE of HMLS LiDAR in the present study was higher than the findings from Liu et al. (2018), who reported a very small RMSE (0.54 m) in tree height using TLS [29]. Primary sources of error in the tree height estimation using HMLS LiDAR technology include the tree crown's top being blocked by itself or neighboring trees, leading to the incorrect identification of the tree top during the segmentation process. Another study pointed out that inaccuracy in tree height measurement with handheld LiDAR arises from certain parts of a taller adjacent tree's crown being wrongly identified as the top of the target tree or mistakes in associating trees during the assessment process [46]. The underestimation of tree height also came from the limited penetration capability of HMLS, leading to missing information at the top of the tree canopy (Figure 5A,D,G,J).

The tree height results from the combined ALS-HMLS were closer to field measurement than those from the HMLS method. This result aligns with previous findings stating that airborne LiDAR can improve the accuracy of tree height [30]. Moreover, Gyawali et al. (2022) reported a strong correlation between field measurement and airborne LiDAR-derived heights, with an RMSE of 1.44 m and a bias of 0.7 m [47]. Wang et al. 2019 found a RMSE of 1.6 m and a bias of -0.96 m in easy plots of a boreal forest in Finland [7]. In past studies, the RMSE and bias increase with tree density increase, highlighting the effect of obstructed understory and dense canopy contributing to uncertainties in tree height estimation, associated with the instability of the field measurements [1,48]. This underscores the necessity to improve the crown delineation algorithm to provide dependable outcomes, especially in dense forest environments and when the trees are taller than 15 m [7,26,49]. Gianetti et al. (2018) highlighted the benefits of merging ALS and HMLS, noting a reduction in RMSE from 2.14 m to 0.94 m and bias moving from -4.61 to -0.3 for both coniferous and broadleaves in Italy [4]. In addition, Sibona et al. (2017) directly measured felled tree height and compared it to LiDAR scanning [18]. The mean absolute difference was 1.04 m for Scots pine, meaning that tree height estimation through LiDAR scanning was closer to actual tree heights than traditional field-based surveys, particularly for tall trees with conical crown shapes. Furthermore, the RMSE of tree height obtained from integrating ALS and HMLS in this study (1.43 m) was much lower than the RMSE of 3.4 m reported in a study by Peng et al. (2022) [50]. Figure 10 illustrates the random positive and negative fluctuations in the estimation of tree height, suggesting that the estimated tree heights derived from the three approaches were generally unbiased.

Overall, ALS effectively measures the height of trees, but it is not suitable for assessing DBH and other attributes near the ground since it primarily captures tree tops and the area above the canopy. On the other hand, HMLS can estimate both the DBH and tree height; however, it often results in underestimations because of thick understory vegetation. In summary, the Integration of ALS and HMLS is considered the most optimal approach for forest inventory purposes (Table 8) as this method maximizes the advantages of each ALS and HMLS method while reducing challenges associated with their application [4].

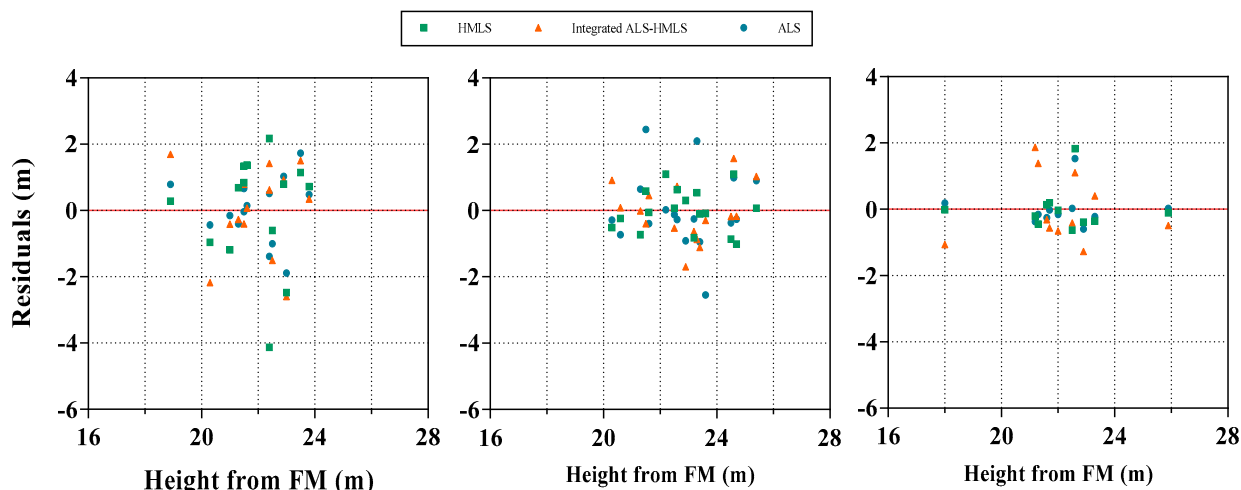


Figure 10. Residual plots of tree height in each plot. Zero lines are highlighted in red.

Table 8. Assessment of the ability to produce accurate DBH and tree height from ALS, HMLS, and Integrated ALS and HMLS compared to field measurement.

LiDAR Approach	Field Measurement	
	DBH	Height
ALS	NA	High
HMLS	High	Medium
Integrated ALS and HMLS	High	High

NA, not available.

Although many previous studies utilize field-based surveys as a standard for assessing LiDAR estimations, tree height accuracy is not strong due to equipment malfunction, the expertise and experience of the surveyors, steep slopes, and dense understory that complicate the identification of tree tops [18]. Additional significant sources of error in DBH also come from measurement inaccuracies and noise, areas with insufficient point density, and branches and trunks that are not circular [44]. The sample plot is square and its edges can lead to inaccuracies in actual tree top identification because of the closed-boundary configuration. Moreover, LiDAR technology often requires high operation costs, including scanning equipment and specialized software. LiDAR’s accuracy may be affected in steep or rocky areas and mixed or multi-layered forests due to its difficulty in distinguishing overlapping crowns. Consequently, additional studies need to incorporate more precise methods for measuring trees in the field to achieve optimal accuracy in tree height calculation in conjunction with LIDAR estimations.

5. Conclusions

This study examined the accuracy of each approach by evaluating point cloud density and found that the combination of ALS and HMLS results in the highest density point clouds, which provide more detailed information about forest stands. High point cloud density enabled more precise measurements of the diameter at breast height (DBH) and tree height, thereby improving the overall accuracy and reliability of forest inventory data obtained from the Integrated ALS and HMLS approach. The results of this study also provide evidence that HMLS offers an accurate and non-destructive estimation of DBH compared to field surveys. In contrast, ALS is a good approach to measure tree height thanks to its ability to capture tree tops and canopy detail, but it is limited in capturing detail under the canopy, specifically tree DBH. Therefore, as a forthcoming

LiDAR application, the combined ALS and HMLS method could transform forest inventory methods, overcoming the challenges of traditional ground-based surveys and enabling faster and more expandable forest evaluations, which contributes to forest ecosystem assessment and carbon stock estimation.

Author Contributions: Conceptualization, M.K., H.B. and L.T.N.T.; methodology, M.K., H.B. and L.T.N.T.; software, L.T.N.T. and H.B.; formal analysis, L.T.N.T.; investigation, L.T.N.T. and H.B.; data curation, L.T.N.T.; writing—original draft preparation, L.T.N.T.; writing—review and editing, L.T.N.T., M.K., B.B.P. and S.-M.C.; visualization, L.T.N.T.; supervision, M.K.; project administration, H.B.; funding acquisition, M.K. and H.B. All authors have read and agreed to the published version of the manuscript.

Funding: This study was carried out with the support of the Development of a K-Forest Management Model based on Stand Characteristics for the Improvement of Ecosystem Service (grant number RS-2022-KF002152) provided by the Korea Forest Service (Korea Forestry Promotion Institute).

Data Availability Statement: The raw data supporting the conclusions of this article will be made available by the authors on request.

Conflicts of Interest: The authors declare no conflicts of interest.

Abbreviations

The following abbreviations are used in this manuscript:

ALS	Airborne Laser Scanning
BMLS	Backpack Mobile Laser Scanning
CHM	Canopy Height Model
DBH	Diameter at Breast Height
DEM	Digital Elevation Model
DSM	Digital Surface Model
FM	Field Measurement
GCPs	Ground Control Points
GNSS	Global Navigation Satellite System
HMLS	Handheld Mobile Laser Scanning
IDW	Inverse Distance Weighting
IMU	Inertial Measurement Unit
LiDAR	Light Detection and Ranging
MAE	Mean Absolute Error
NIFS	National Institute of Forest Science
RGB	Red Green Blue
RMSE	Root Mean Square Error
SLAM	Simultaneous Localization and Mapping
SOR	Statistical Outlier Removal
TLS	Terrestrial Laser Scanning
UAV	Unmanned Aerial Vehicle

References

1. Hyyppä, E.; Yu, X.; Kaartinen, H.; Hakala, T.; Kukko, A.; Vastaranta, M.; Hyyppä, J. Comparison of Backpack, Handheld, under-Canopy UAV, and above-Canopy UAV Laser Scanning for Field Reference Data Collection in Boreal Forests. *Remote Sens.* **2020**, *12*, 3327. [[CrossRef](#)]
2. White, J.C.; Coops, N.C.; Wulder, M.A.; Vastaranta, M.; Hilker, T.; Tompalski, P. Remote Sensing Technologies for Enhancing Forest Inventories: A Review. *Can. J. Remote Sens.* **2016**, *42*, 619–641. [[CrossRef](#)]
3. Ghimire, S.; Xystrakis, F.; Koutsias, N. Using Terrestrial Laser Scanning to Measure Forest Inventory Parameters in a Mediterranean Coniferous Stand of Western Greece. *PGF J. Photogramm. Remote Sens. Geoinf. Sci.* **2017**, *85*, 213–225. [[CrossRef](#)]

4. Giannetti, F.; Puletti, N.; Quatrini, V.; Travaglini, D.; Bottalico, F.; Corona, P.; Chirici, G. Integrating Terrestrial and Airborne Laser Scanning for the Assessment of Single-Tree Attributes in Mediterranean Forest Stands. *Eur. J. Remote Sens.* **2018**, *51*, 795–807. [[CrossRef](#)]
5. Ma, K.; Xiong, Y.; Jiang, F.; Chen, S.; Sun, H. A Novel Vegetation Point Cloud Density Tree-Segmentation Model for Overlapping Crowns Using UAV LiDAR. *Remote Sens.* **2021**, *13*, 1442. [[CrossRef](#)]
6. Shimizu, K.; Nishizono, T.; Kitahara, F.; Fukumoto, K.; Saito, H. Integrating Terrestrial Laser Scanning and Unmanned Aerial Vehicle Photogrammetry to Estimate Individual Tree Attributes in Managed Coniferous Forests in Japan. *Int. J. Appl. Earth Obs. Geoinf.* **2022**, *106*, 102658. [[CrossRef](#)]
7. Wang, Y.; Lehtomäki, M.; Liang, X.; Pyörälä, J.; Kukko, A.; Jaakkola, A.; Liu, J.; Feng, Z.; Chen, R.; Hyypä, J. Is Field-Measured Tree Height as Reliable as Believed—A Comparison Study of Tree Height Estimates from Field Measurement, Airborne Laser Scanning and Terrestrial Laser Scanning in a Boreal Forest. *ISPRS J. Photogramm. Remote Sens.* **2019**, *147*, 132–145. [[CrossRef](#)]
8. Xie, Y.; Zhang, J.; Chen, X.; Pang, S.; Zeng, H.; Shen, Z. Accuracy Assessment and Error Analysis for Diameter at Breast Height Measurement of Trees Obtained Using a Novel Backpack LiDAR System. *For. Ecosyst.* **2020**, *7*, 33. [[CrossRef](#)]
9. Bauwens, S.; Bartholomeus, H.; Calders, K.; Lejeune, P.; Hyypä, J.; Liang, X.; Puttonen, E. Forest Inventory with Terrestrial LiDAR: A Comparison of Static and Hand-Held Mobile Laser Scanning. *Forests* **2016**, *7*, 127. [[CrossRef](#)]
10. Bazezew, M.N.; Hussin, Y.A.; Kloosterman, E.H. Integrating Airborne LiDAR and Terrestrial Laser Scanner Forest Parameters for Accurate Above-Ground Biomass/Carbon Estimation in Ayer Hitam Tropical Forest, Malaysia. *Int. J. Appl. Earth Obs. Geoinf.* **2018**, *73*, 638–652. [[CrossRef](#)]
11. Hauglin, M.; Lien, V.; Næsset, E.; Gobakken, T. Geo-Referencing Forest Field Plots by Co-Registration of Terrestrial and Airborne Laser Scanning Data. *Int. J. Remote Sens.* **2014**, *35*, 3135–3149. [[CrossRef](#)]
12. Yang, B.; Zang, Y.; Dong, Z.; Huang, R. An Automated Method to Register Airborne and Terrestrial Laser Scanning Point Clouds. *ISPRS J. Photogramm. Remote Sens.* **2015**, *109*, 62–76. [[CrossRef](#)]
13. Liang, X.; Kankare, V.; Hyypä, J.; Wang, Y.; Kukko, A.; Haggrén, H.; Yu, X.; Kaartinen, H.; Jaakkola, A.; Guan, F.; et al. Terrestrial Laser Scanning in Forest Inventories. *ISPRS J. Photogramm. Remote Sens.* **2016**, *115*, 63–77. [[CrossRef](#)]
14. Novotny, J.; Navratilova, B.; Albert, J.; Cienciala, E.; Fajmon, L.; Brovkina, O. Comparison of Spruce and Beech Tree Attributes from Field Data, Airborne and Terrestrial Laser Scanning Using Manual and Automatic Methods. *Remote Sens. Appl.* **2021**, *23*, 2352–9385. [[CrossRef](#)]
15. Carson, W.W.; Andersen, H.-E.; Reutebuch, S.E.; Mcgaughey, R.J. Lidar applications in forestry—an overview. In Proceedings of the ASPRS Annual Conference, Denver, CO, USA, 23–28 May 2004.
16. Cheng, L.; Chen, S.; Liu, X.; Xu, H.; Wu, Y.; Li, M.; Chen, Y. Registration of Laser Scanning Point Clouds: A Review. *Sensors* **2018**, *18*, 1641. [[CrossRef](#)]
17. Fekry, R.; Yao, W.; Cao, L.; Shen, X. Ground-Based/UAV-LiDAR Data Fusion for Quantitative Structure Modeling and Tree Parameter Retrieval in Subtropical Planted Forest. *For. Ecosyst.* **2022**, *9*, 100065. [[CrossRef](#)]
18. Sibona, E.; Vitali, A.; Meloni, F.; Caffo, L.; Dotta, A.; Lingua, E.; Motta, R.; Garbarino, M. Direct Measurement of Tree Height Provides Different Results on the Assessment of LiDAR Accuracy. *Forests* **2016**, *8*, 7. [[CrossRef](#)]
19. Chehreh, B.; Moutinho, A.; Viegas, C. Latest Trends on Tree Classification and Segmentation Using UAV Data—A Review of Agroforestry Applications. *Remote Sens.* **2023**, *15*, 2263. [[CrossRef](#)]
20. Choi, H.; Song, Y. Comparing Tree Structures Derived among Airborne, Terrestrial and Mobile LiDAR Systems in Urban Parks. *Glsci Remote Sens.* **2022**, *59*, 843–860. [[CrossRef](#)]
21. Hilker, T.; van Leeuwen, M.; Coops, N.C.; Wulder, M.A.; Newnham, G.J.; Jupp, D.L.B.; Culvenor, D.S. Comparing Canopy Metrics Derived from Terrestrial and Airborne Laser Scanning in a Douglas-Fir Dominated Forest Stand. *Trees Struct. Funct.* **2010**, *24*, 819–832. [[CrossRef](#)]
22. Koch, B.; Heyder, U.; Welnacker, H. Detection of Individual Tree Crowns in Airborne Lidar Data. *Photogramm. Eng. Remote Sens.* **2006**, *72*, 357–363. [[CrossRef](#)]
23. Lindberg, E.; Holmgren, J. Individual Tree Crown Methods for 3D Data from Remote Sensing. *Curr. For. Rep.* **2017**, *3*, 19–31. [[CrossRef](#)]
24. Zhou, X.; Ma, K.; Sun, H.; Li, C.; Wang, Y.; Zhou, X.; Ma, K.; Sun, H.; Li, C.; Wang, Y. Estimation of Forest Stand Volume in Coniferous Plantation from Individual Tree Segmentation Aspect Using UAV-LiDAR. *Remote Sens.* **2024**, *16*, 2736. [[CrossRef](#)]
25. Douss, R.; Farah, I.R. Extraction of Individual Trees Based on Canopy Height Model to Monitor the State of the Forest. *Trees For. People* **2022**, *8*, 100257. [[CrossRef](#)]
26. Latella, M.; Sola, F.; Camporeale, C. A Density-Based Algorithm for the Detection of Individual Trees from LiDAR Data. *Remote Sens.* **2021**, *13*, 322. [[CrossRef](#)]
27. Del Perugia, B.; Giannetti, F.; Chirici, G.; Travaglini, D. Influence of Scan Density on the Estimation of Single-Tree Attributes by Hand-Held Mobile Laser Scanning. *Forests* **2019**, *10*, 277. [[CrossRef](#)]

28. Ryding, J.; Williams, E.; Smith, M.J.; Eichhorn, M.P. Assessing Handheld Mobile Laser Scanners for Forest Surveys. *Remote Sens.* **2015**, *7*, 1095–1111. [[CrossRef](#)]
29. Liu, G.; Wang, J.; Dong, P.; Chen, Y.; Liu, Z. Estimating Individual Tree Height and Diameter at Breast Height (DBH) from Terrestrial Laser Scanning (TLS) Data at Plot Level. *Forests* **2018**, *9*, 398. [[CrossRef](#)]
30. Ojoatse, S.; Zhang, C.; Hussin, Y.A.; Kloosterman, H.E.; Ismail, M.H. Assessing the Uncertainty of Tree Height and Aboveground Biomass from Terrestrial Laser Scanner and Hypsometer Using Airborne LiDAR Data in Tropical Rainforests. *IEEE J. Sel. Top. Appl. Earth Obs. Remote Sens.* **2019**, *12*, 4149–4159. [[CrossRef](#)]
31. Holopainen, M.; Vastaranta, M.; Hyypä, J. Outlook for the Next Generation’s Precision Forestry in Finland. *Forests* **2014**, *5*, 1682–1694. [[CrossRef](#)]
32. National Institute of Forest Science (NIFS). *Practical Forest Measurement and Survey*; National Institute of Forest Science (NIFS): Seoul, Republic of Korea, 2018.
33. Vatandaşlar, C.; Zeybek, M. Extraction of Forest Inventory Parameters Using Handheld Mobile Laser Scanning: A Case Study from Trabzon, Turkey. *Measurement* **2021**, *177*, 109328. [[CrossRef](#)]
34. Li, W.; Guo, Q.; Jakubowski, M.K.; Kelly, M. A New Method for Segmenting Individual Trees from the Lidar Point Cloud. *Photogramm. Eng. Remote Sens.* **2012**, *78*, 75–84. [[CrossRef](#)]
35. Balsa Barreiro, J.; Avariento Vicent, J.P.; Lerma García, J.L. Airborne Light Detection and Ranging (LiDAR) Point Density Analysis. *Sci. Res. Essays* **2012**, *7*, 3010–3019. [[CrossRef](#)]
36. Jia, Y.; Lan, T.; Peng, T.; Wu, H.; Li, C.; Ni, G. Effects of Point Density on DEM Accuracy of Airborne LiDAR. In Proceedings of the 2013 IEEE International Geoscience and Remote Sensing Symposium—IGARSS, Melbourne, VIC, Australia, 21–26 July 2013; pp. 493–496. [[CrossRef](#)]
37. Petras, V.; Petrasova, A.; McCarter, J.B.; Mitsova, H.; Meentemeyer, R.K. Point Density Variations in Airborne Lidar Point Clouds. *Sensors* **2023**, *23*, 1593. [[CrossRef](#)]
38. Puetz, A.M.; Olsen, R.C.; Anderson, B. Effects of Lidar Point Density on Bare Earth Extraction and DEM Creation. *Laser Radar Technol. Appl. XIV* **2009**, 7323, 126–133. [[CrossRef](#)]
39. LaRue, E.A.; Fahey, R.; Fuson, T.L.; Foster, J.R.; Matthes, J.H.; Krause, K.; Hardiman, B.S. Evaluating the Sensitivity of Forest Structural Diversity Characterization to LiDAR Point Density. *Ecosphere* **2022**, *13*, e4209. [[CrossRef](#)]
40. Liu, X.; Zhang, Z.; Peterson, J.; Chandra, S. The Effect of LiDAR Data Density on DEM Accuracy. In Proceedings of the 17th International Congress on Modelling and Simulation (MODSIM07), Australia, New Zealand, 10–13 December 2007.
41. Singh, K.K.; Chen, G.; McCarter, J.B.; Meentemeyer, R.K. Effects of LiDAR Point Density and Landscape Context on Estimates of Urban Forest Biomass. *ISPRS J. Photogramm. Remote Sens.* **2015**, *101*, 310–322. [[CrossRef](#)]
42. Panagiotidis, D.; Abdollahnejad, A.; Slavík, M. 3D Point Cloud Fusion from UAV and TLS to Assess Temperate Managed Forest Structures. *Int. J. Appl. Earth Obs. Geoinf.* **2022**, *112*, 102917. [[CrossRef](#)]
43. Lee, Y.; Woo, H.; Lee, J.S. Forest Inventory Assessment Using Integrated Light Detection and Ranging (LiDAR) Systems: Merged Point Cloud of Airborne and Mobile Laser Scanning Systems. *Sens. Mater.* **2022**, *34*, 4583–4597. [[CrossRef](#)]
44. Krooks, A.; Kaasalainen, S.; Kankare, V.; Joensuu, M.; Raunonen, P.; Kaasalainen, M. Predicting Tree Structure from Tree Height Using Terrestrial Laser Scanning and Quantitative Structure Models. *Silva Fenn.* **2014**, *48*, 1125. [[CrossRef](#)]
45. Choi, S.W.; Kim, T.G.; Kim, J.P.; Kim, S.J. Assessment on the Applicability of a Handheld LiDAR for Measuring the Geometric Structures of Forest Trees. *J. Korean Assoc. Geogr. Inf. Stud.* **2022**, *25*, 48–58. [[CrossRef](#)]
46. Olofsson, K.; Holmgren, J.; Olsson, H. Tree Stem and Height Measurements Using Terrestrial Laser Scanning and the RANSAC Algorithm. *Remote Sens.* **2014**, *6*, 4323–4344. [[CrossRef](#)]
47. Gyawali, A.; Aalto, M.; Peuhkurinen, J.; Villikka, M.; Ranta, T. Comparison of Individual Tree Height Estimated from LiDAR and Digital Aerial Photogrammetry in Young Forests. *Sustainability* **2022**, *14*, 3720. [[CrossRef](#)]
48. Vatandaşlar, C.; Seki, M.; Zeybek, M. Assessing the Potential of Mobile Laser Scanning for Stand-Level Forest Inventories in near-Natural Forests. *For. An. Int. J. For. Res.* **2023**, *96*, 448–464. [[CrossRef](#)]
49. Mielcarek, M.; Stereńczak, K.; Khosravipour, A. Testing and Evaluating Different LiDAR-Derived Canopy Height Model Generation Methods for Tree Height Estimation. *Int. J. Appl. Earth Obs. Geoinf.* **2018**, *71*, 132–143. [[CrossRef](#)]
50. Peng, X.; Zhao, A.; Chen, Y.; Chen, Q.; Liu, H. Tree Height Measurements in Degraded Tropical Forests Based on UAV-LiDAR Data of Different Point Cloud Densities: A Case Study on *Dacrydium Pierrei* in China. *Forests* **2021**, *12*, 328. [[CrossRef](#)]

Disclaimer/Publisher’s Note: The statements, opinions and data contained in all publications are solely those of the individual author(s) and contributor(s) and not of MDPI and/or the editor(s). MDPI and/or the editor(s) disclaim responsibility for any injury to people or property resulting from any ideas, methods, instructions or products referred to in the content.